JOURNAL OF GUIDANCE, CONTROL, AND DYNAMICS
Vol. 25, No. 1, January–February 2002

Aeroservoelastic Structural and Control Optimization Using Robust Design Schemes

Boris Moulin,* Moshe Idan,† and Mordechay Karpel‡
Technion—Israel Institute of Technology, 32000 Haifa, Israel

The procedure for structural and robust control design of multi-input/multi-output aeroservoelastic systems presented contains modeling of uncertainties, synthesis of a robust controller, and a unified structural and control optimization process under stress, flutter, and control performance constraints. Robust control design techniques can enhance the preliminary structural design for cases where certain system parameters are not known exactly or are uncertain. An aeroservoelastic interaction module is used for mediation between the structural optimization code and the control synthesis tools in an iterative coupled process. It provides the reduced-size state-space aeroelastic models needed for control synthesis, including model sensitivities to structural uncertainties, and integrates the resulting control model in structural optimization that includes robust-control considerations in terms of singular value constraints. The efficient uncertainty modeling developed is based on the readily available structural sensitivity data and the linear fractional transformation tools. Modeling of inertial uncertainties of the controlled structure was performed to account for relatively large inertial deviations of a fighter aircraft wing-tip missile. The numerical example clearly demonstrates the effectiveness of the proposed design scheme and its usefulness at preliminary design stages of aircraft with multiple external store loads.

Nomenclature

$[A_{(.)}]$, $[B_{(.)}]$, $[C_{(.)}]$, $[D_{(.)}]$	=	state-space matrices
$\left[\frac{A}{C}\middle\vert\frac{B}{D}\right]$	=	$[C][s[I]-[A]]^{-1}[B]+[D]$
$[A_{h1,2,3}]$, $[D]$, $[E]$	=	rational aerodynamic approximation matrices
b	=	reference semichord
$[DM]$	=	sensitivity of the modal mass matrix to a normalized uncertainty
$\mathcal{F}_\ell$	=	lower linear fractional transformation (LFT)
$[G_v]$	=	controller gain matrix
$[I]$	=	identity matrix
k	=	maximum relative mass perturbation
$[L_i]$, $[L_o]$	=	multi-input/multi-output input and output uncertainty matrices
$\mathcal{M}^l$	=	LFT matrix for linear uncertainty
$\mathcal{M}^q$	=	LFT matrix for quadratic uncertainty
$[M_{hc}]$	=	mass coupling matrix between control and structural modes
$[M_{hh}]$, $[B_{hh}]$, $[K_{hh}]$	=	modal mass, viscous damping, and stiffness matrices
$[\bar{M}_{hh}]$, $[\tilde{M}_{hh}]$	=	nominal and perturbed modal mass matrices
m	=	mass of a perturbed part of the structure
n_a	=	number of aerodynamic states
n_c	=	number of control surfaces
n_h	=	number of generalized displacements
n_s	=	number of sensors
q	=	dynamic pressure
$[R]$	=	aerodynamic lag matrix
s	=	Laplace transform variable
V	=	true air speed
$W_{(.)}$	=	weighting functions of controller design
$\{x\}$, $\{u\}$, $\{y\}$	=	state, input, and output vectors
$\{x_a\}$	=	aerodynamic augmented states
$\{x_{\mathrm{ac}}\}$	=	vector of actuator states
$[\Delta M_{hh}]$	=	variation of modal mass matrix
Δm	=	mass variation
$\{\delta\}$	=	normalized uncertainty
$\{\delta_c\}$	=	control-surface deflections
$\{\xi\}$	=	generalized displacements
$\underline{\sigma}\{\cdot\}$	=	minimum singular value
$\{\phi_g\}$	=	normal modes
ω	=	frequency

Subscripts

ac	=	actuators
ae	=	open-loop aeroelastics
ase	=	closed-loop aeroservoelastics
c	=	control modes or controller
h	=	structural modes
p	=	open-loop aeroelastics with actuators
v	=	gain-open aeroservoelastic system

Presented as Paper 2000-1453 at the AIAA/ASME/ASCE/AHS/ASC 41st Structures, Structural Dynamics, and Materials Conference, Atlanta, GA, 3–6 April 2000; received 8 May 2000; revision received 15 November 2000; accepted for publication 17 November 2000.

*Research Associate, Faculty of Aerospace Engineering. Member AIAA.
†Senior Lecturer, Faculty of Aerospace Engineering. Associated Fellow AIAA.
‡Professor, Faculty of Aerospace Engineering. Senior Member AIAA.

I. Introduction

THE aeroservoelastic coupling between the aerodynamics, structural dynamics, and control systems of flight vehicles must be taken into account in procedures for optimal aircraft design. A given aerodynamic layout requires the optimization of the structural design variables and parameters of the control system, while simultaneously accounting for stress, flutter, and control performance constraints.[1]

ASTROS[2] was developed to provide a multidisciplinary analysis and design capability for aerospace structures. The disciplines considered include structural and aeroelastic (AE) analysis. A new aeroservoelastic (ASE) discipline was recently incorporated into ASTROS,[1] which allows simultaneous optimization of the structural and control systems. The ASE discipline is based on the AE state-space equations of motion obtained using rational function approximation of the unsteady aerodynamic force coefficient matrices and a control system that is defined in a way that allows the modeling of most general linear control laws in the ASE loop.

The state-space ASE formulation facilitated the use of modern control analysis and synthesis methods. Robust-control μ-analysis

techniques were applied in ASE analysis by Lind and Brenner.[3,4] They showed how model uncertainties can be modeled and used for calculation of robust stability margins. Their applications were mainly in the context of flight-test stability evaluation.

The main objective of the current study is to develop an efficient technique for reliable modeling of the AE system variations caused by uncertainties in the physical properties of its structural elements and to apply this methodology in modeling the effects of inertial uncertainties and perturbations of the aircraft for preliminary design and analysis. This goal is accomplished by incorporating the new ASE computational module[1] in a robust multi-input/multi-output (MIMO) control design scheme based on the μ-synthesis approach and by the evaluation of the performance of this new capability using realistic design studies. The robustness of the resulting control system is utilized to address ASE model uncertainties and variations in the design and optimization process.

The AE equations of motion and their presentation in state-space form are summarized in the next section. Then, the procedure of structural and control optimization of MIMO uncertain systems is discussed. New formulations for modeling of inertial uncertainties of the controlled ASE structure based on the structural sensitivity data and using the linear fractional transformation technique are presented next. This modeling procedure is then applied to a sample aircraft model with uncertainties in its tip-store inertial properties, followed by a design of a robust roll-rate controller and structural and control optimization. The numerical example is instrumental in demonstrating the effectiveness of the proposed multidisciplinary design procedure.

II. ASE System Equations

The ASE formulation in this paper follows the state-space formulation of Refs. 1 and 5. The time-domain ASE models for stability and response analysis are constructed from the separate models of the AE plant and the control system expressed in a state-space form. The control system includes the control surfaces driven by actuators, sensors related to the structural degrees of freedom, and a linear MIMO control law that relates the actuator inputs to the sensor signals. The formulation of the AE equations of motion in a state-space form is based on expressing the aerodynamic force coefficient matrices as rational functions of the Laplace variable s, using either Roger's approximation[6] or the minimum-state method of Karpel.[7] The open-loop ASE model is a result of the augmentation of the AE model and the state-space realization of the actuators, which leads to the plant equations

$$\{\dot{x}_p\} = [A_p]\{x_p\} + [B_p]\{u_p\} \tag{1a}$$

$$\{y_p\} = [C_p]\{x_p\} \tag{1b}$$

where $\{u_p\}$ is the vector of actuator inputs and $\{y_p\}$ is the vector of sensor signals.

The vector of the plant states $\{x_p\}$ includes the vectors of n_h generalized displacements $\{\xi\}$ and n_h velocities $\{\dot{\xi}\}$, vector $\{x_a\}$ of n_a aerodynamic states, and vector $\{x_{ac}\}$ of $3n_c$ actuator states. The ASE modeling procedure assumes that the order of each actuator is at least three, with the number of poles larger than the number of zeros by at least three.[7] In the plant model of Eq. (1a), a control surface i is driven by a basic third-order actuator whose states are δ_{c_i}, $\dot{\delta}_{c_i}$, and $\ddot{\delta}_{c_i}$, where δ_{c_i} is the vector of actuator output displacements expressed in radians, namely, the hypothetical control-surface rotation if there were no structural dynamic effects. The associated control-surface deflection, with the rest of the aircraft not moving, is called control mode. The assembly of basic actuator states $\{x_{ac}\}$ contains the subassemblies δ_{c_i}, $\dot{\delta}_{c_i}$, and $\ddot{\delta}_{c_i}$. This representation yields the strictly proper form of Eq. (1), with no direct effect of $\{u_p\}$ on $\{y_p\}$. Higher-order actuator dynamics can be expressed by adding proper transfer functions in series, as part of the control system that will be addressed later.

The matrix $[A_p]$ may be written according to the components $\{\xi\}$, $\{\dot{\xi}\}$, $\{x_a\}$, and $\{x_{ac}\}$ of the vector $\{x_p\}$ as

$$[A_p] = [\bar{M}_p]^{-1}[\bar{A}_p] \tag{2}$$

where

$$[\bar{M}_p] = \begin{bmatrix} [I] & 0 & 0 & 0 \\ 0 & [\bar{M}] & 0 & 0 \\ 0 & 0 & [I] & 0 \\ 0 & 0 & 0 & [I] \end{bmatrix}$$

$$\begin{bmatrix} \bar{A}_p \end{bmatrix} = \begin{bmatrix} 0 & [I] & 0 & 0 \\ \bar{A}_{12} & \bar{A}_{22} & \bar{A}_{23} & \bar{B}_{ae}^{(2)} \\ 0 & E_h & (V/b)R & B_{ae}^{(3)} \\ 0 & 0 & 0 & A_{ac} \end{bmatrix}$$

$$[\bar{M}] = [M_{hh}] + (qb^2/V^2)\begin{bmatrix} A_{hh_2} \end{bmatrix}, \qquad \bar{A}_{12} = -\begin{bmatrix} K_{hh} + qA_{hh_0} \end{bmatrix}$$

$$\bar{A}_{22} = -\begin{bmatrix} B_{hh} + (qb/V)A_{hh_1} \end{bmatrix}, \qquad \bar{A}_{23} = -q[D]$$

$$\bar{B}_{ae}^{(2)} = \begin{bmatrix} -q\begin{bmatrix} A_{hc_0} \end{bmatrix} & -(qb/V)\begin{bmatrix} A_{hc_1} \end{bmatrix} & -\begin{bmatrix} M_{hc} + (qb^2/V^2)A_{hc_2} \end{bmatrix} \end{bmatrix}$$

$$B_{ae}^{(3)} = [0 \quad [E_c] \quad 0]$$

$[M_{hh}]$, $[B_{hh}]$, and $[K_{hh}]$ are the modal mass, viscous damping, and stiffness matrices; $[M_{hc}]$ is the mass coupling matrix between the control and structural modes; $[A_{hh_{0,1,2}}]$, $[A_{hc_{0,1,2}}]$, $[D]$, $[E_{h,c}]$, and $[R]$ are the rational aerodynamic approximation matrices; b is the reference semichord; V is the true air speed; and q is the dynamic pressure.

Next, the ASE interaction model is formulated to handle any linear time-invariant control system and enables changes in its parameters during a multidisciplinary design and optimization. The ASE model and the fixed part of the controller, which is not changed in the optimization process, are combined into the so-called gain-open ASE model

$$\{\dot{x}_v\} = [A_v]\{x_v\} + [B_v]\{u_v\} \tag{3a}$$

$$\{y_v\} = [C_v]\{x_v\} + [D_v]\{u_v\} \tag{3b}$$

The closed-loop ASE model is obtained using output feedback by relating the input vector $\{u_v\}$ to the output vector $\{y_v\}$ via the variable gain matrix $[G_v]$, which may be changed during the design process,

$$\{u_v\} = [G_v]\{y_v\} \tag{4}$$

The resulting closed-loop ASE equations of motion are

$$\{\dot{x}_{ase}\} = [A_{ase}]\{x_{ase}\} \tag{5}$$

with

$$[A_{ase}] = [A_v] + [B_v][G_v][I - D_vG_v]^{-1}[C_v]$$

The closed-loop state-space realization of the ASE system is used in an optimization scheme that computes the flutter, stability margins, and robust performance constraints and that utilizes the sensitivities of these constraints to changes in the structural design variables and in the control gains.

III. Structural and Control Optimization of MIMO Uncertain Systems

The procedure of multidisciplinary structural and control optimization developed in Ref. 1 presents an efficient tool for highly coupled structural and control aircraft design, which simultaneously complies with structural (stress/strain, static aeroelastic, flutter, and dynamic response) and control (stability and performance) design requirements.

MIMO stability margins and sensitivities were defined, following Ref. 8, by introducing ASE system uncertainties at the plant input or output as described in Fig. 1. The input and output MIMO stability

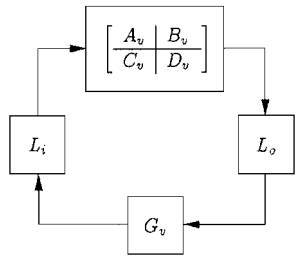

Fig. 1 MIMO stability margin evaluation setup.

margins are defined with respect to uncertainties (variations) in the matrices $[L_i]$ and $[L_o]$, which are assumed to be diagonal, that is,

$$[L_i] = \text{diag}\left[g_l^i e^{j\phi_l^i}\right], \qquad l = 1, 2, \ldots, N_i \tag{6a}$$

$$[L_o] = \text{diag}\left[g_k^o e^{j\phi_k^o}\right], \qquad k = 1, 2, \ldots, N_o \tag{6b}$$

where N_i and N_o are the number of inputs and outputs, respectively, to the ASE model. At the nominal condition, $g_l^i = g_k^o = 1$ and $\phi_l^i = \phi_k^o = 0 \ \ \forall\, l, k$, that is, $[L_i] = I_{N_i \times N_i}$ and $[L_o] = I_{N_o \times N_o}$.

Sufficient conditions for a guaranteed gain margin $\bar{g}^i$ and phase margin $\bar{\phi}^i$ at any input to the gain-open ASE plant are[8]

$$[(1 - 1/\bar{g}^i)^2 + 2(1 - \cos\bar{\phi}^i)/\bar{g}^i]^{\frac{1}{2}} < \underline{\sigma}\{I - G_v P_v\} \tag{7a}$$

or

$$[(1 - \bar{g}^i)^2 + 2\bar{g}^i(1 - \cos\bar{\phi}^i)]^{\frac{1}{2}} < \underline{\sigma}\left\{I - [G_v P_v]^{-1}\right\} \tag{7b}$$

where

$$[P_v(s)] = [C_v][sI - A_v]^{-1}[B_v] + [D_v]$$

and $\underline{\sigma}\{\cdot\}$ is the minimum singular value of the argument matrix evaluated at $s = j\omega \ \forall \ \omega \geq 0$. Sufficient conditions for output gain and phase margins are similar to the inequalities of Eqs. (7), except those of replacing the $[G_v P_v]$ terms with $[P_v G_v]$. Sensitivities of these stability margins are readily incorporated in the ASE module.

In this paper, the multidisciplinary design and optimization procedure of Ref. 1 is extended to handle MIMO ASE systems with model uncertainties. The main design steps are as follows:

1) The design of a baseline structure can be obtained by the optimization of an initial structure with static and/or open-loop flutter constraints only.

2) With regards to the modeling of the baseline system uncertainties, clearly, the uncertainty model depends on the baseline system characteristics and the variable parameters. The modeling should be realistic, that is, parametric, to reduce overbounding and, thus, over-design.

3) Robust control synthesis using the baseline system and the uncertainty model for a prespecified design point (velocity and dynamic pressure) is aimed at satisfying the basic robust stability and additional robust closed-loop performance requirements. The results of this control synthesis step determine the following design stages.

4) If the controller synthesis is successful (i.e., all of the robust stability and performance requirements are met), a multidisciplinary optimization of the closed-loop system is performed to guarantee flutter margins and control performance for a range of velocity and dynamic pressure values outside the control design point. If the design is satisfactory, quit the procedure; if not, repeat step 3 with the new optimized structure.

5) If the control synthesis is not successful (i.e., the control system obtained in step 3 does not comply with all of the robust stability and performance requirements), the designer has to modify the baseline structure or the design specifications. One way would be to reduce the uncertainty range. Alternatively, a closed-loop optimization of the baseline structure with the control system of step 3 can be carried out to obtain a modified structure. The latter was found to be most efficient in actual design examples. The optimization is carried out using the following guidelines and constraints:

a) Flutter constraints guarantee closed-loop system stability.

b) Single input/single output and MIMO stability margins together with additional low-frequency control constraints must be tightened compared to the baseline design to obtain an improved structure.

c) Additional, for example, static, constraints can be introduced, although most often the design specifications and constraints of step 1 can be retained.

6) It can be anticipated that the structure obtained in the preceding step will be heavier than the initial one. In this case the obtained structure is used as the new baseline for step 3, where a new robust controller for the new system is synthesized. If the structure was not changed in the optimization and the required constraints were satisfied just by modifying the changeable part of the control system, the control design of step 3 should be repeated with the initial baseline structure and modified control design specifications, guided by the findings of step 5.

This procedure enables the inclusion of various structural and robust-control synthesis schemes in a common aircraft design loop. The control design results in a controller that provides the best performance and stability margins with respect to structural perturbations of a given structure and defines the control parameters that can be tuned during the subsequent structural optimization. This procedure can be repeated several times, providing a common framework for interaction between structures and control specialists. The ASE system uncertainty modeling and a related design scenario for a sample aircraft are presented in the subsequent sections.

IV. Model of the Inertial Uncertainties

Modeling of the ASE system uncertainty is based on its sensitivity data and the linear fractional transformation tools. The novel procedure developed here can easily handle a variety of model uncertainties, including variations in the structural and inertial properties, uncertainties in the aerodynamic data, and more. As an example, in this study we consider only uncertainties in the inertial properties of the controlled structure. The inertial variations are expressed in terms of changes in the mass, moments of inertia, and position of the centers of gravity of lumped parts of the structure. This is a typical design problem for aircraft with external stores. Inertial variations were not treated in previous robust ASE works,[4] mainly because of the modeling complexity that arises from the inversion of the mass matrix $[\tilde{M}_{hh}]$ in Eq. (2). These perturbations lead to deviation of the modal mass matrix $[M_{hh}]$ from its nominal, that is,

$$[\tilde{M}_{hh}] = [\bar{M}_{hh}] + [\Delta M_{hh}] \tag{8}$$

where $[\bar{M}_{hh}]$ is the nominal matrix and $[\Delta M_{hh}]$ is its variation caused by the model uncertainty. We adopt the fixed-basis modal approach, which assumes that the structural displacements of the perturbed system can be adequately expressed as a linear combination of the baseline normal modes. Whereas the baseline matrix $[\bar{M}_{hh}]$ is diagonal, the variation $[\Delta M_{hh}]$ is not. Fictitious-mass techniques[9] can be used to allow large local mass changes with a fixed modal basis. In this work, however, because the mass perturbations are added to already-large lumped inertial properties of a tip store, fictitious masses are not required.

We analyze the contribution of local mass and moment of inertia variations to the ASE model uncertainty without changing the centers of mass of the lumped elements. Because of the linear dependence of the global finite element mass matrix on the local masses and moment of inertia, the modal mass matrix variation is also linear in those parameters and is expressed as

$$[\Delta M_{hh}] = \frac{\partial[M_{hh}]}{\partial m}\Delta m \tag{9}$$

where m is the mass (or moment of inertia) of the disturbed part of the structure and Δm is the actual variation in the mass (or moment of inertia).

The derivative $\partial[M_{hh}]/\partial m$ is obtained by pre- and postmultiplication of the sensitivity of the global finite element mass matrix $[M_{gg}]$ by the normal modes $[\phi_g]$:

$$\frac{\partial[M_{hh}]}{\partial m} = [\phi_g]^T \frac{\partial[M_{gg}]}{\partial m}[\phi_g] \tag{10}$$

With the relations of Eqs. (9) and (10), Eq. (8) becomes

$$[\tilde{M}_{hh}] = [\bar{M}_{hh}] + [DM]\delta \tag{11}$$

where $\delta \in [-1, 1]$ is the normalized uncertainty and $[DM]$ is the sensitivity of the modal mass matrix to δ expressed as

$$[DM] = \frac{\partial [M_{hh}]}{\partial m} k\bar{m} \tag{12}$$

Here $\bar{m}$ is the nominal mass (or moment of inertia) of the perturbed part of the structure, and k is the ratio between the maximum mass perturbation and the nominal mass $\bar{m}$, that is, $-k\bar{m} \le \Delta m \le k\bar{m}$.

Equation (11) can be cast in the form of a lower linear fractional transformation (LFT) (see, for example, Ref. 10) as

$$[\tilde{M}_{hh}] = \mathcal{F}_\ell(\mathcal{M}^l, \Delta) = \mathcal{M}^l_{11} + \mathcal{M}^l_{12}\Delta\left(I - \mathcal{M}^l_{22}\Delta\right)^{-1}\mathcal{M}^l_{21} \tag{13}$$

where

$$\mathcal{M}^l = \begin{bmatrix} \mathcal{M}^l_{11} & \mathcal{M}^l_{12} \\ \mathcal{M}^l_{21} & \mathcal{M}^l_{22} \end{bmatrix} = \begin{bmatrix} \bar{M}_{hh} & DM \\ I_h & 0 \end{bmatrix}$$

$$\Delta = [I_h]\delta$$

where the superscript l denotes the linear uncertainties.

The dependence of the modal mass matrix on variations or uncertainty in the centers of gravity of lumped mass elements is quadratic. For example, an offset Δx in the x direction between a structural grid point and the center of gravity of the mass lumped to this point leads to a deviation of the grid point mass matrix $[M_{\text{gp}}]$ as follows:

$$[\Delta M_{\text{gp}}] \triangleq [A_1]\Delta x + [A_2]\Delta x^2$$

$$= \begin{bmatrix} 0 & 0 & 0 & 0 & 0 & 0 \\ 0 & 0 & 0 & 0 & 0 & m\Delta x \\ 0 & 0 & 0 & 0 & -m\Delta x & 0 \\ 0 & 0 & 0 & 0 & 0 & 0 \\ 0 & 0 & -m\Delta x & 0 & m\Delta x^2 & 0 \\ 0 & m\Delta x & 0 & 0 & 0 & m\Delta x^2 \end{bmatrix} \tag{14}$$

In general, for any normalized variation $\delta \in [-1, 1]$ in the center of gravity the relation is

$$[\tilde{M}_{hh}] = [\bar{M}_{hh}] + \left[DM^{(1)}\right]\delta + \left[DM^{(2)}\right]\delta^2 \tag{15}$$

where

$$\left[DM^{(i)}\right] = [\phi_g]^T[A_i][\phi_g]e_{\text{cg}} \tag{16}$$

and $e_{\text{cg}} = \max(\Delta x)$.

Equation (15) can be expressed as an LFT

$$[\tilde{M}_{hh}] = \mathcal{F}_\ell(\mathcal{M}^q, \Delta) \tag{17}$$

where

$$\mathcal{M}^q_{11} = [\bar{M}_{hh}], \qquad \mathcal{M}^q_{12} = \begin{bmatrix} DM^{(1)} & DM^{(2)} \end{bmatrix}$$

$$\mathcal{M}^q_{21} = \begin{bmatrix} I_h \\ 0 \end{bmatrix}, \qquad \mathcal{M}^q_{22} = \begin{bmatrix} 0 & 0 \\ I_h & 0 \end{bmatrix}$$

$$\Delta = [I_{2h}]\delta$$

For any n_u uncertainties in the ASE system, the modal mass matrix is constructed as a sum of LFTs

$$[\tilde{M}_{hh}] = \mathcal{F}_\ell(\mathcal{M}, \Delta) \tag{18}$$

where

$$\mathcal{M}_{11} = [\bar{M}_{hh}], \qquad \mathcal{M}_{12} = \begin{bmatrix} \mathcal{M}^1_{12} & \mathcal{M}^2_{12} & \cdots & \mathcal{M}^{n_u}_{12} \end{bmatrix}$$

$$\mathcal{M}_{21} = \begin{bmatrix} \mathcal{M}^1_{21} \\ \mathcal{M}^2_{21} \\ \vdots \\ \mathcal{M}^{n_u}_{21} \end{bmatrix}, \qquad \mathcal{M}_{22} = \operatorname{diag}\left(\mathcal{M}^1_{22}, \mathcal{M}^2_{22}, \ldots, \mathcal{M}^{n_u}_{22}\right)$$

$$\Delta = \operatorname{diag}\left([I]\delta_1, [I]\delta_2, \ldots, [I]\delta_{n_u}\right)$$

Every linear uncertainty inserts matrices $\mathcal{M}_{ij}$ of the form given by Eq. (13), and uncertainties with quadratic dependence insert matrices of the form given by Eq. (17). The identity matrices in the expression for the Δ matrix are of order n_h for linear uncertainties and $2n_h$ for quadratic.

The derived model of the modal mass matrix is used next to construct the uncertainty model of the ASE system equations of motion. In particular, the mass matrix $[\bar{M}_p]$ of Eqs. (1a) and (2) depends on the modal mass matrix $[\tilde{M}_{hh}]$. Therefore, the model of $[\bar{M}_p]$ with uncertainties can be easily expressed as an LFT of the model uncertainties

$$[\tilde{M}_p] = \mathcal{F}_\ell(\bar{\mathcal{M}}, \Delta) \tag{19}$$

where

$$\bar{\mathcal{M}}_{11} = [\bar{M}_p], \qquad \bar{\mathcal{M}}_{12} = \begin{bmatrix} 0 \\ \mathcal{M}_{12} \\ 0 \\ 0 \end{bmatrix}$$

$$\bar{\mathcal{M}}_{21} = \begin{bmatrix} 0 & \mathcal{M}_{21} & 0 & 0 \end{bmatrix}, \qquad \bar{\mathcal{M}}_{22} = \mathcal{M}_{22}$$

The matrix product $[\bar{M}_p]^{-1}[\bar{A}_p]$ is also an LFT, leading to the following equation of motion

$$\{\dot{x}_p\} = \mathcal{F}_\ell(\bar{\mathcal{N}}, \Delta)\{x_p\} + [B_p]\{u_p\} \tag{20}$$

where

$$\bar{\mathcal{N}} = \begin{bmatrix} \bar{\mathcal{M}}^{-1}_{11}\bar{A}_p & -\bar{\mathcal{M}}^{-1}_{11}\bar{\mathcal{M}}_{12} \\ \bar{\mathcal{M}}_{21}\bar{\mathcal{M}}^{-1}_{11}\bar{A}_p & \bar{\mathcal{M}}_{22} - \bar{\mathcal{M}}_{21}\bar{\mathcal{M}}^{-1}_{11}\bar{\mathcal{M}}_{12} \end{bmatrix}$$

$$= \begin{bmatrix} A_p & -\bar{\mathcal{M}}^{-1}_{11}\bar{\mathcal{M}}_{12} \\ \bar{\mathcal{M}}_{21}A_p & \bar{\mathcal{M}}_{22} - \bar{\mathcal{M}}_{21}\bar{\mathcal{M}}^{-1}_{11}\bar{\mathcal{M}}_{12} \end{bmatrix}$$

Perturbation of the modal mass matrix also affects the equation of the plant outputs in the case of acceleration measurements, where the $[C_p]$ matrix becomes

$$[C_p] = [\phi_y][\bar{M}]^{-1}\begin{bmatrix} \bar{A}_{12} & \bar{A}_{22} & \bar{A}_{23} & \bar{B}^{(2)}_{\text{ae}} \end{bmatrix} = [\phi_y][\bar{M}]^{-1}\begin{bmatrix} \bar{A}^{(2)}_p \end{bmatrix} \tag{21}$$

where $[\phi_y]$ is the row vector of modal displacements at the sensor location. With the preceding models of the mass matrix uncertainties, the output equation can be expressed as

$$\{y_p\} = \mathcal{F}_\ell(\bar{\mathcal{N}}^O, \Delta)\{x_p\} \tag{22}$$

where

$$\bar{\mathcal{N}}^O = \begin{bmatrix} C_p & -[\phi_y]\bar{\mathcal{M}}^{-1}_{11}\bar{\mathcal{M}}_{12} \\ \bar{\mathcal{M}}_{21}A_p & \bar{\mathcal{M}}_{22} - \bar{\mathcal{M}}_{21}\bar{\mathcal{M}}^{-1}_{11}\bar{\mathcal{M}}_{12} \end{bmatrix}$$

Note that $\bar{\mathcal{N}}^O_{21} = \bar{\mathcal{N}}_{21}$ and $\bar{\mathcal{N}}^O_{22} = \bar{\mathcal{N}}_{22}$.

Finally, after opening the uncertainty Δ block loop and performing some elementary LFT operations, the model of the uncertain ASE system is expressed as

$$\{\dot{x}_p\} = [A_p]\{x_p\} + [B_1]\{u_\delta\} + [B_p]\{u_p\} \tag{23a}$$

$$\{y_\delta\} = [C_1]\{x_p\} + [D_{11}]\{u_\delta\} \tag{23b}$$

$$\{y_p\} = [C_p]\{x_p\} + [D_{21}]\{u_\delta\} \tag{23c}$$

where $[B_1] = \bar{\mathcal{N}}_{12}$, $[C_1] = \bar{\mathcal{N}}_{21}$, $[D_{11}] = \bar{\mathcal{N}}_{22}$, and $[D_{21}] = \bar{\mathcal{N}}^{o}_{12}$ and $\{u_\delta\}$ and $\{y_\delta\}$ represent, respectively, the inputs and outputs of the uncertainty block. The transfer function matrix for the overall augmented plant becomes

$$P(s) = \left[\begin{array}{c|cc} A_p & B_1 & B_p \\ \hline C_1 & D_{11} & 0 \\ C_p & D_{21} & 0 \end{array}\right] \tag{24}$$

The preceding procedure may result in a repeated scalar uncertainty block of a relatively large dimension. Because the dimension and, thus, complexity of a controller synthesized using design techniques such as μ depends on the size of the uncertainty block, it is desirable to reduce it to a minimum. In the repeated scalar uncertainty case, this can be accomplished using minimum realization techniques, as is discussed in Ref. 11. There, if the repeated scalar block variable is interpreted as the Laplace s variable, the size minimization procedure is equivalent to obtaining a minimum state-space realization of a dynamic system.[11] This procedure leads to a minimum dimensional uncertainty block representation only when the Δ contains one repeated scalar block. If the uncertainty is modeled by a few repeated scalar blocks, the same procedure can be repeated for each block, but no minimum can be guaranteed. In any case, the reduction of the uncertainty block Δ is extremely desirable, leading to a simplified design.

The modeling procedure presented demonstrates the efficient use of the LFT tools for modeling a wide variety of ASE model uncertainties, assuming their dependence on the physical system parameters is rational. This type of dependence was encountered while modeling uncertainties in the system inertial properties. The modeling procedure can deal efficiently with the difficulties associated with the mass matrix inversion in the ASE model and with the quadratic dependence on the variations in the lumped-element center of gravity. Complex rational dependence may lead to repeated scalar block uncertainty models, as is the case when considering modal mass perturbations.

V. Test-Case Aircraft Model

The uncertainty modeling and multidisciplinary design procedure presented is tested using the AE model of a generic advanced fighter aluminum (AFA) aircraft. The finite element ASTROS model has an all-movable horizontal tail and four control surfaces on each wing, where only the two trailing-edge control surfaces are used for maneuvering. The aircraft structural model is shown in Fig. 2. The skin of the wing torsion box is subject to structural optimization. A top view of the wing box divided into 13 design zones is shown in Fig. 3. The design variables are the thickness of the upper and lower aluminum skins in the 13 design zones, leading to a total of 26 structural design variables. More details on this model may be found in Ref. 12, where the model is optimized for minimum weight, with only stress and static AE constraints.

The unsteady aerodynamic model of AFA is shown in Fig. 4. The model consists of nine aerodynamic panels representing the fuselage, inboard and outboard parts of the wing, four control surfaces, a tip missile, and a horizontal tail. The panels representing the fuselage and the horizontal tail are attached to the support grid point of the structural model. Four root boxes of the inboard LEF panel are also attached to this point. Wing, control surfaces, and missile panels are splined to the structural grid points.

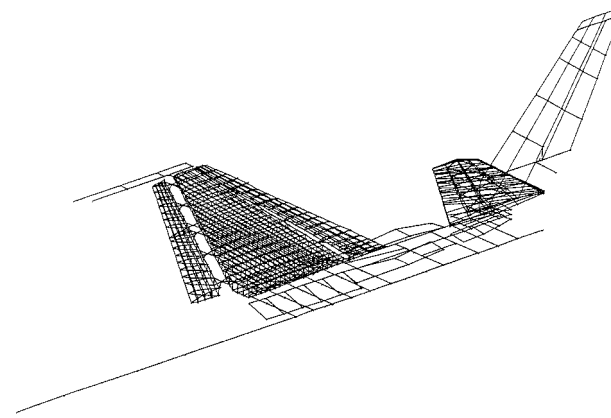

Fig. 2 AFA structural model.

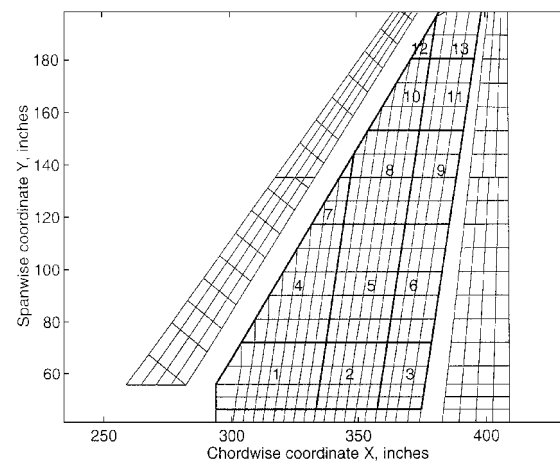

Fig. 3 AFA wing structural model.

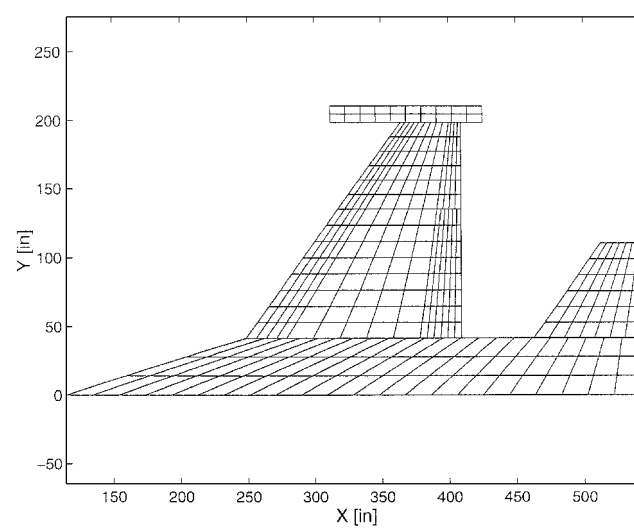

Fig. 4 Unsteady aerodynamic model.

VI. Model of Uncertainty due to Tip-Store Inertial Deviations

In the numerical example we tackle the uncertainties in the inertial properties of the AFA wing-tip store, a wing-tip missile. The missile inertial properties are represented in ASTROS by a concentrated mass element attached to a grid point located at the nominal missile c.g. Uncertainties of three inertial properties of the tip missile are considered in this study: the total mass, the pitch moment of

inertia about c.g., and the c.g. location in the x-axis direction. These uncertainties are expressed as

$$\Delta m_z = m_z - \bar{m}_z = \bar{m}_z k_z \delta_1 \tag{25a}$$

$$\Delta I_{yy} = I_{yy} - \bar{I}_{yy} = \bar{I}_{yy} k_{yy} \delta_2 \tag{25b}$$

$$\Delta x_{\mathrm{cg}} = x_{\mathrm{cg}} - \bar{x}_{\mathrm{cg}} = e_{\mathrm{cg}} \delta_3 \tag{25c}$$

where m_z, I_{yy}, and x_{cg} are, respectively, the missile mass, moment of inertia, and c.g. x coordinate, with $\bar{m}_z$, $\bar{I}_{yy}$, and $\bar{x}_{\mathrm{cg}}$ representing their nominal values. Here k_z and k_{yy} are the maximal relative uncertainties in m_z and I_{yy}, and e_{cg} is the maximum displacement of c.g. from its nominal position; $\delta_i \in [-1, 1]$ are the normalized uncertainties.

Because of the linear dependence of the modal mass matrix on m_z and I_{yy}, these uncertainties are modeled according to Eqs. (10–12). The effects of mass changes are considered only in the z (vertical) direction, assuming that the in-plane mass-change effects are negligible. Because the mass variations in z-axis direction, as well as the moment of inertia I_{yy}, lead to changes only in a single element of the global mass matrix of the finite element model, the pre- and postmultiplications in Eq. (10) can be performed using only one row of the mode matrix $[\phi_g]$. The quadratically dependent c.g. variations are modeled according to Eqs. (14–16).

The overall state-space model and the transfer function matrix of AFA with uncertainties are obtained according to Eqs. (23) and (24), leading to an uncertainty matrix Δ that consists of two n_h repeated scalar blocks and one $2n_h$ repeated scalar block. The size of Δ is reduced to six using the technique of Ref. 11 with two scalar blocks and one repeated scalar block of four.

VII. Controller Design

The interconnection model used in the robust controller design is presented in Fig. 5. It incorporates the AFA ASE dynamics model with its uncertainties Δ, performance specification functions, and design constraints. The latter are specified using the various weighting functions $W_{(\cdot)}$. The synthesis results in a dynamic controller $K(s)$.

The main design goal is to provide robust stability and level-one roll-rate performance of the AFA in compliance with MIL-STD.[13] This is dictated in the design with the reference model

$$W_{\mathrm{ref}}(s) = \frac{2.076}{(0.2s+1)(0.27s+1)} \tag{26}$$

This model assures 20% better than high-speed level-one roll-rate performance, defined by the time it takes the aircraft to reach various roll angles: 90 deg in 1.4 s, 180 deg in 2.3 s, and 360 deg in 4.1 s. The allowable difference between this desired reference model and the actual aircraft response is specified by

$$W_e(s) = 5/(0.08s+1) \tag{27}$$

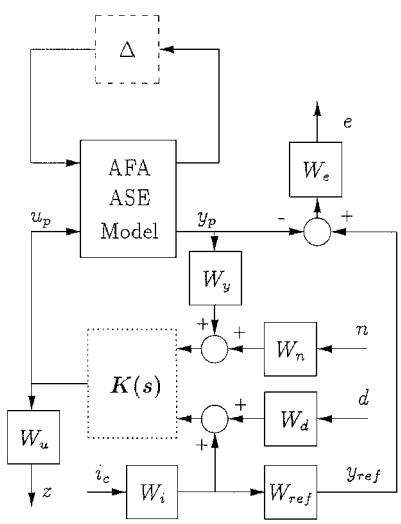

Fig. 5 Robust-control design interconnection model.

requiring a roll-rate error lower that 10% of its maximum reference value in the frequency range of up to 2 Hz. Together with the slight overdesign requirement in the specified reference model, this will assure level-one roll performance.

The normalized pilot roll command is bandlimited to about 1 Hz, specified by the W_i weight

$$W_i(s) = \frac{(0.01s+1)}{(0.2s+1)} \tag{28}$$

The inputs to the controller are the measured pilot commands and the measured aircraft roll rate. Both signals are assumed to be contaminated with additive white measurement noise with power spectral densities specified by the constants W_d and W_n. In addition, an integral control action is obtained by introducing the weighting function (approximate integration)

$$W_y(s) = \frac{(0.002s+1)}{(100s+1)} \tag{29}$$

acting on the measured roll rate.

Finally, the aileron deflection angles used for the roll maneuver were limited by setting the actuator weighting function W_u to the reciprocal of a realistic limit of 13 deg of aileron deflection.

VIII. Numerical Results

The preliminary structural design was aimed to provide a baseline for consequent robust control design and closed-loop optimization. The design was initiated with a basic structural model with uniform thickness of 0.5 in. assigned to all of the design skin elements, with a total weight of 779.5 lb. Stress and open-loop flutter constraints were applied in the first optimization run. The stresses were calculated for a single symmetric 9 g pull-up maneuver at Mach 0.95. The von Mises stresses of the skin elements were constrained to less than 36,700 psi. The flutter constraints were applied for antisymmetric boundary conditions at Mach 0.9. There were 30 low-frequency modes, including 1 rigid-body mode, used for updating the modal properties and performing ASE analysis during the optimization. There were 13 reduced frequency values between 0.0 and 0.29 used to generate the aerodynamic data base. The nominal design velocity was defined as 12,057 in./s. Flutter design points were defined at seven velocity values of 9000; 10,000; 11,000; 12,057; 13,000; 14,000; and 14,470 in./s. Two additional velocity values were used to provide the required flutter margins. The structural damping was set to $g = 0.02$ and was converted to generalized viscous damping matrix using $[B_{hh}] = g[\omega_h]$, where $[\omega_h]$ is the diagonal matrix of natural frequencies. The flutter constraints required positive damping at all of the design points.

The optimization performed in ASTROS employed the modal-based static disciplines described in Refs. 12 and 14 and the ASE module. The total weight of the wing box skin was reduced to 486.8 lb. The resulting structure was then used as the baseline for the robust controller design.

The state-space model of the baseline structure at the design velocity of 12,057 in./s was constructed next by the ASE module of ASTROS. It included 40 structural states, representing 20 low-frequency modes (including 1 rigid-body roll mode), 10 aerodynamic states, and 6 actuator states, representing the 2 trailing-edge aileron actuators, leading to a total of 56 states. The inputs were the commands u_{p_1} and u_{p_2} to the outboard and inboard wing trailing-edge actuators, respectively. The only output y_p was the roll-rate reading. The state-space matrices $[A_p]$, $[B_p]$, and $[C_p]$ of that model were stored in a data file, which was then exported into the MATLAB® environment for consequent control design. In addition, the data files also included the sensitivity matrices of the preceding model to variations (uncertainties) in the system's physical parameters. These sensitivities are used in the MATLAB code to construct the overall system uncertainty model.

The uncertainties of the tip missile mass and the moment of inertia were bounded to ±30% of their nominal values, and the uncertainty of the tip missile center of gravity was bounded to ±10 in. First, a full uncertainty model of the system was constructed. Then, the order of each of the mass and the moment of inertia uncertainty

blocks was reduced from 20 to 1, whereas the order of the center of gravity uncertainty block was reduced from 40 to 4.

The interconnection model of Fig. 5 was used for a μ-controller synthesis using the MATLAB μ-Analysis and Synthesis Toolbox.[15] The sparse structure of the uncertainty block motivated the use of μ synthesis, which has the potential of less conservative designs in such structured uncertainty cases. The design process converged after 8 D-K iterations, with a structured singular value of $\mu = 1.18$. The 205th order controller was order reduced using the balanced truncation technique to 47, with negligible effect on the value of μ. The structured singular value plot shown in Fig. 6 demonstrates the violation of the requirement for $\mu \leq 1$, indicating that the robust performance specifications were not met.

To reach the required performance, the baseline structure had to be modified. The state-space model of the μ controller was written by the MATLAB code in the bulk-data format of ASTROS. Within ASTROS, the controller was connected to the ASE model through two additional design gains on the controller output. The resulting closed-loop model was then subjected to multidisciplinary optimization where structural properties and the two additional gains can change simultaneously. The baseline values of these control gains were $G_1 = 1$ and $G_2 = 1$, with magnitude limits of $\pm 20\%$. The same stress and flutter constraints as in the preliminary structural design were applied together with additional control related constraints. In particular, constraints on the minimum singular values of the closed-loop system (for MIMO robustness) and on the total dc gain of the open-loop system were introduced. The latter constraints were increased by about 10% compared to their values in the baseline structure. As before, 30 low-frequency modes were used in the optimization process.

The optimization weight history is shown in Fig. 7. All of the constraints were satisfied by increasing the structural weight to 505.1 lb

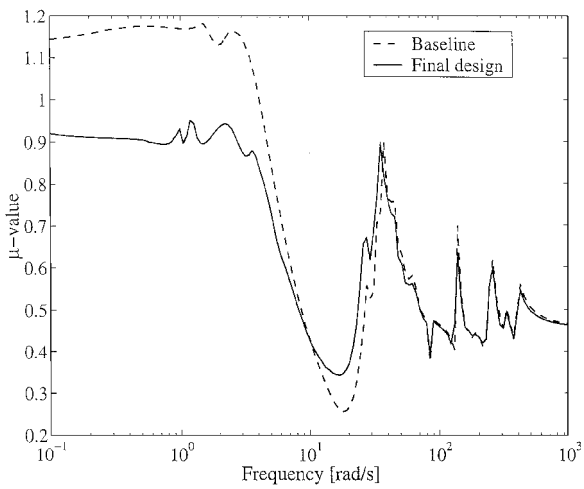

Fig. 6 Structured singular value.

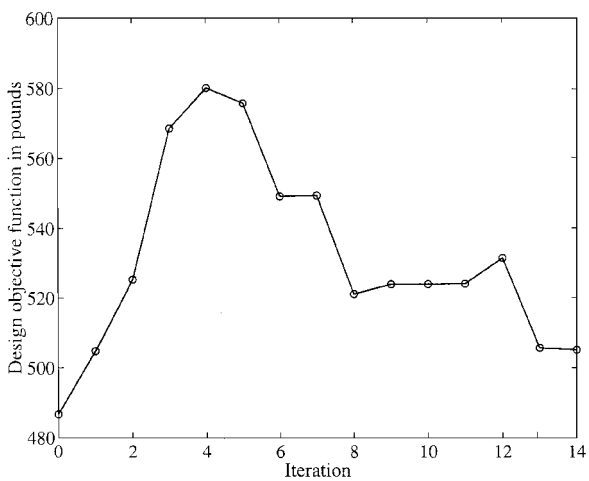

Fig. 7 Optimization weight history.

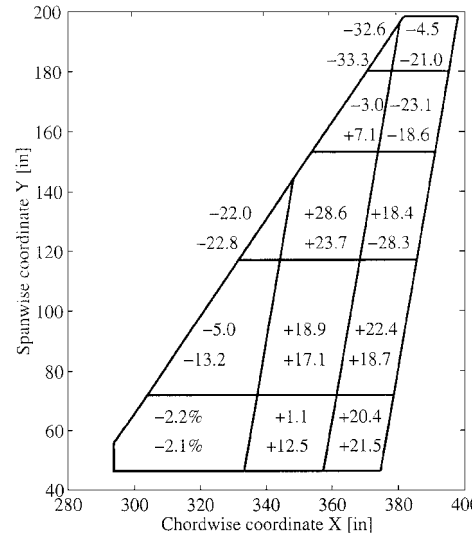

Fig. 8 Thickness changes (in percent) of wing box skin for structural zones (upper number is for upper skin, lower number for lower skin).

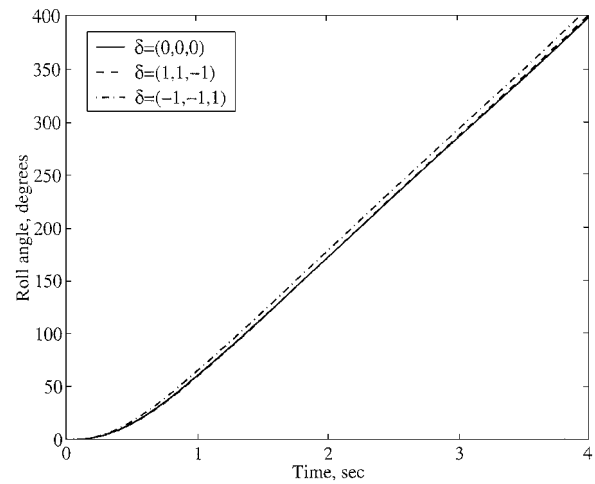

Fig. 9 Roll response to step command.

and slightly changing the overall controller gains to $G_1 = 0.985$ and $G_2 = 0.933$. Changes in the structural design variables for each zone are shown in Fig. 8. The increase in the weight and the minor reduction in the controller gains show that the performance requirements cannot be achieved just by controller redesign and require modifications of the structure. To satisfy the addition singular value constraints, the structure weight was increased leading to a decrease in the required controller gains (due to increase in the AE control effectiveness).

The second μ controller was designed for the modified structure. The design process converged after 5 D-K iterations, with a structured singular value of $\mu = 0.93$ and a 171st-order controller. Again, the controller order was reduced to 40 with a negligible effect on the structured singular value, as shown in Fig. 6.

The roll angle response of the final AFA design to a step command input for the extreme uncertainty values is shown in Fig. 9. The uncertainty cases of $\delta = (1, 1, 1)$, $\delta = (1, -1, 1)$, and $\delta = (-1, -1, -1)$ demonstrate very similar response as the nominal system [$\delta = (0, 0, 0)$]. In addition, the $\delta = (-1, 1, 1)$ case demonstrates almost an identical response as the $\delta = (-1, -1, 1)$ case. For all of the cases, a roll angle of 90 deg is reached in about 1.3 s, 180 deg in 2.1 s, and 360 deg in 3.6 s, all faster than the level-one requirements.[13]

IX. Conclusions

A methodology for modeling ASE system uncertainty is developed. This methodology provides a tool for constructing an

uncertain or parameter-variable ASE system model while minimizing the uncertainty overbounding. The concept and procedure for robust ASE design of MIMO uncertain systems presented in this study facilitate an efficient multidisciplinary design optimization process that incorporates modern methods of robust-control synthesis and analysis. The effectiveness of the proposed procedure relies on the efficient transfer of data, constraints, and requirements between the various disciplines involved. In addition, efficiency is obtained by a reliable and compact modeling of the ASE system uncertainties. The combination of the overall design procedure and the uncertainty modeling tools lead to ASE systems that satisfy both stress and AE requirements, as well as robust stability and robust closed-loop performance requirements. This was clearly demonstrated using a realistic test case design of a fighter aircraft with tip-missile (store) inertial uncertainties. The adequate modeling and robust design process over relatively large deviations of the store mass, moments of inertia, and c.g. location can be very useful at preliminary ASE design stages of an aircraft capable of carrying a large variety of external stores.

Acknowledgments

This work was supported in part by the U.S. Air Force Research Laboratories/Air Vehicles under a Small Business Technology Transfer Phase II contract through Zona Technology and the University of Oklahoma, by the Israeli Ministry of Immigrant Absorption, and by the Fund for the Promotion of Research at Technion—Israel Institute of Technology.

References

[1]Idan, M., Karpel, M., and Moulin, B., "Aeroservoelastic Interaction Between Aircraft Structural and Control Design Schemes," *Journal of Guidance, Control, and Dynamics*, Vol. 22, No. 4, 1999, pp. 513–519.

[2]Neill, D. J., Johnson, E. H., and Confield, R., "ASTROS-A Multidisciplinary Automated Structural Design Tool," *Journal of Aircraft*, Vol. 27, No. 12, 1990, pp. 1021–1027.

[3]Lind, R., and Brenner, M., "Incorporating Flight Data into a Robust Aeroelastic Model," *Journal of Aircraft*, Vol. 35, No. 3, 1998, pp. 470–477.

[4]Lind, R., and Brenner, M., *Robust Aeroservoelastic Stability Analysis*, Springer-Verlag, London, 1999, pp. 67–113.

[5]Karpel, M., "Reduced-Order Models for Integrated Aeroservoelastic Optimization," *Journal of Aircraft*, Vol. 36, No. 1, 1999, pp. 146–155.

[6]Roger, K. L., "Airplane Math Modeling Methods for Active Control Design," *Proceedings of the 44th AGARD Structures and Materials Panel*, AGARD-CP-228, April 1977, pp. 4.1–4.11.

[7]Karpel, M., "Time-Domain Aeroservoelastic Modeling Using Weighted Unsteady Aerodynamic Forces," *Journal of Guidance, Control, and Dynamics*, Vol. 13, No. 1, 1990, pp. 30–37.

[8]Mukhopadhyay, V., "Control Law Synthesis and Stability Robustness Improvement Using Constrained Optimization Techniques," *Control and Dynamic Systems*, Vol. 32, Academic, New York, 1990, pp. 163–205.

[9]Karpel, M., and Raveh, D., "Fictitious Mass Element in Structural Dynamics," *AIAA Journal*, Vol. 34, No. 3, 1996, pp. 607–613.

[10]Zhou, K., Doyle, J. C., and Glover, K., *Robust and Optimal Control*, Prentice–Hall, Upper Saddle River, NJ, 1996, pp. 247–269.

[11]Idan, M., and Shaviv, G. E., "Robust Control Design Strategy with Parameter Dominated Uncertainty," *Journal of Guidance, Control, and Dynamics*, Vol. 19, No. 3, 1996, pp. 605–611.

[12]Karpel, M., Moulin, B., and Love, M. H., "Modal-Based Structural Optimization with Static Aeroelastic and Stress Constraints," *Journal of Aircraft*, Vol. 34, No. 3, 1997, pp. 433–440.

[13]"Military Standard. Flying Qualities of Piloted Aircraft," U.S. Air Force MIL-STD-1797A, 30 Jan. 1990, pp. 436, 437.

[14]Karpel, M., Moulin, B., and Love, M. H., "Structural Optimization with Static Constraints Using Extendible Modal Basis," *AIAA Journal*, Vol. 37, No. 11, 1999, pp. 1514–1519.

[15]Balas, G. J., Doyle, J. C., Glover, K., Packard, A., and Smith, R., "μ-Analysis and Synthesis Toolbox for Use with MATLAB. User's Guide. Version 3," MathWorks, Inc., Natick, MA, 1998, pp. 5.1–5.16.